Supracrystals

DOI: 10.1002/anie.201408675

Counterion-Assisted Shaping of Nanocluster Supracrystals**

Qiaofeng Yao, Yue Yu, Xun Yuan, Yong Yu, Dan Zhao, Jianping Xie, and Jim Yang Lee**

Abstract: *Ag_{44}(p-MBA)$_{30}^{4-}$ (p-MBA = para-mercaptobenzoic acid) nanocluster (NC) supracrystals (SCs) with customizable shapes can be obtained by simply altering the type and concentration of the counterions of the p-MBA ligands in the dimethylsulfoxide (DMSO)/water crystallization system. Changing the counterion of the p-MBA ligand from H^+ to Cs^+ eliminates the directional hydrogen bonds in the SCs, resulting in the packing of deprotonated Ag_{44}(p-MBA)$_{30}^{4-}$ NCs into octahedral SCs, which is in stark contrast to the rhombohedral SCs that were formed by the packing of protonated Ag_{44}(p-MBA)$_{30}^{4-}$ NCs in previous studies. Furthermore, the double layer of deprotonated Ag_{44}(p-MBA)$_{30}^{4-}$ NCs is sensitive to charge screening induced by increasing the Cs^+ concentration, thereby providing a means to regulate the precipitation kinetics of the Ag_{44}(p-MBA)$_{30}^{4-}$ NCs for SC shape engineering. Slow precipitation kinetics was found to favor over-growth at the corners and edges of the octahedral SC nuclei, shaping the SCs into concave octahedra.*

Thiolate-protected noble-metal nanoclusters (NCs) or $M_n(SR)_m$ (e.g., M = Au or Ag) are ultrasmall (< 2 nm) nanoparticles with molecule-like properties, such as quantized charging, strong luminescence, and enhanced catalytic activity.[1] The crystallization of $M_n(SR)_m$ NCs is central to the development of cluster chemistry,[1a,2] because the determination of the NC structure demands very high quality supracrystals (SCs) of the NCs.[2a,b,3] Aside from size, shape is another attribute that can affect the physicochemical (e.g., optical and catalytic) properties of crystalline materials through geometry, symmetry, and the exposure of selected crystallographic faces.[4] The reciprocity between shape and property has been regularly shown by metal nanocrystals,[4a,b,5] and a diversity of shapes for the SCs may likewise increase the versatility of SCs in various applications. The formation of SCs from NC building blocks under shape control, however, is technically challenging. Thus far, only rhombohedral or needle-like NC-SCs with monoclinic, triclinic, or orthorhombic crystal symmetry have been reported.[2a,c,3,6] Therefore, the crystallization of NCs into shape-tailorable SCs with a structural diversity similar to that of nanocrystals is clearly of interest to the cluster research community. The ability to perform shape engineering can accelerate NC structural determination by X-ray crystallography (through the packing of NCs into SCs of high symmetry)[7] and also the development of reliable property–shape relationships for NC-SCs.[8]

Recently, Desireddy et al. reported the synthesis of rhombohedral Ag_{44}(*p*-MBA)$_{30}^{4-}$ NC-SCs (*p*-MBA = *para*-mercaptobenzoic acid).[2b] As the SCs were grown from NCs with the protonated form of the *p*-MBA ligands, the crystal habit (e.g., the rhombohedral shape of the SCs) is strongly related to the binding environment established by the directional hydrogen bonds (H-bonds) of the NC components.[9] Herein, we demonstrate that the shape of Ag_{44}(*p*-MBA)$_{30}^{4-}$ NC-SCs can be tailored by altering the binding environment of the NC components (e.g., from directional to non-directional by the elimination of H-bonds). A simple change of the *p*-MBA ligand counterions from H^+ to non-H^+ cations (e.g., Cs^+) changes the shape of the Ag_{44}(*p*-MBA)$_{30}^{4-}$ NC-SCs from rhombohedral with D_{3d} symmetry[2b] to octahedral with the higher O_h symmetry. Furthermore, the high charge density of the Ag_{44}(*p*-MBA)$_{30}^{4-}$ NCs developed by deprotonating the *p*-MBA ligands offers a means to modify the SC growth kinetics by charge-screening effects, which could be used to obtain octahedral Ag_{44}(*p*-MBA)$_{30}^{4-}$ NC-SCs with either convex or concave faces.

The synthesis of Ag_{44}(*p*-MBA)$_{30}^{4-}$ NCs was based on the method of Desireddy et al.[2b] with some minor modifications (for details, see the Supporting Information). The as-synthesized raw Ag_{44}(*p*-MBA)$_{30}^{4-}$ NCs showed well-defined absorption peaks at 415, 485, 538, 645 and 835 nm, which are identical to the characteristic absorption features of Ag_{44}(*p*-MBA)$_{30}^{4-}$ NCs (Supporting Information, Figure S1 a),[2b,c,10] which is an indication of the high purity of the synthesized material. The transmission electron microscopy (TEM) image (Figure S1 b) of the as-synthesized Ag_{44}(*p*-MBA)$_{30}^{4-}$ NCs shows that the Ag core size was < 2 nm.

Contrary to the previously reported crystallization of protonated Ag_{44}(*p*-MBA)$_{30}^{4-}$ NCs in a single-solvent system (dimethylformamide, DMF), the crystallization of deprotonated Ag_{44}(*p*-MBA)$_{30}^{4-}$ NCs (with Cs^+ counterions) in this study was carried out in a dual-solvent system where a good solvent (e.g., water) was used to increase the solubility of the deprotonated Ag_{44}(*p*-MBA)$_{30}^{4-}$ NCs in a solvent mixture containing a bad solvent (e.g., dimethylsulfoxide, DMSO). The selection of the good/bad solvent pair was based on vapor pressure differences where the good solvent should possess a higher vapor pressure (i.e., evaporate more easily) than the bad one. Slow and selective evaporation of the good solvent could then occur to induce the crystallization of the Ag_{44}(*p*-MBA)$_{30}^{4-}$ NCs.

[*] Q. Yao, Dr. Y. Yu, Dr. X. Yuan, Dr. Y. Yu, Prof. D. Zhao, Prof. J. Xie, Prof. J. Y. Lee
Department of Chemical and Biomolecular Engineering
National University of Singapore
10 Kent Ridge Crescent, Singapore 119260 (Singapore)
E-mail: chexiej@nus.edu.sg
cheleejy@nus.edu.sg

[**] We acknowledge financial support from the Ministry of Education through Academic Research Grants R279-000-349-112 and R279-000-409-112. Q.Y. thanks the National University of Singapore for a research scholarship.

Supporting information for this article is available on the WWW under http://dx.doi.org/10.1002/anie.201408675.

Experimentally, the raw $Ag_{44}(p\text{-MBA})_{30}^{4-}$ NCs were first pelletized by centrifugation in the presence of ethanol, followed by washing with a CsOH aqueous solution (66 mM) thrice to fully deprotonate the *p*-MBA ligands (for details, see the Supporting Information). The deprotonated $Ag_{44}(p\text{-MBA})_{30}^{4-}$ NCs were redissolved in a DMSO/water mixture (NC concentration, [NC] = 0.73 mM) containing a predetermined concentration of Cs^+ ([Cs^+], from the dissociation of dissolved CsOH). The solution was then placed in a vacuum oven (ca. 20 mbar and 40 °C) to remove the water. After one to three days of growth (with the duration depending on the volume fraction of DMSO or X_{DMSO} in the dual-solvent system), the $Ag_{44}(p\text{-MBA})_{30}^{4-}$ NC-SCs were recovered as a black–red precipitate at the bottom of the crystallization tube.

In stark contrast to the protonated $Ag_{44}(p\text{-MBA})_{30}^{4-}$ NCs, which formed rhombohedral SCs,[2b] the Cs^+-deprotonated $Ag_{44}(p\text{-MBA})_{30}^{4-}$ NCs were packed into SCs with an octahedral shape at [Cs^+] = 33 mM and X_{DMSO} = 0.5 (Figure 1a). The as-fabricated SCs encompassed a broad size distribution (Figure 1a, top inset) with an average diameter of 24.48 μm (from counting > 100 SCs). The regular octahedral morphology (Figure 1a, bottom insets) of the SCs suggests them to be single-crystalline SCs with O_h symmetry, a symmetry characteristic of the cubic crystal system, which was not found in other reported NC-SC systems. The octahedral morphology is congruent with face-centered-cubic (fcc) SCs enclosed by the $(111)_{SC}$ facets, as confirmed by a powder X-ray diffraction pattern where the most dominant $(111)_{SC}$ peak was located at $2\theta \approx 4.19°$ (calculated value: 4.20°; see Figure S2 for the calculation details). We propose that the formation of the octahedral SCs was thermodynamically driven. After complete elimination of the directional H-bonds, the interaction between the Cs^+-deprotonated $Ag_{44}(p\text{-MBA})_{30}^{4-}$ NCs should be non-directional, and therefore, their packing may be approximated by the classic hard-sphere model. The hard-sphere model suggests that the depletion force (entropic effect) could drive the packing of the spheres into the most compact pattern (e.g., fcc packing).[11] The exposure of the $(111)_{SC}$ facets in a fcc SC is predicted upon the minimization of the surface energy (see Figure S2 for a detailed discussion).[8d,12] The formation of octahedral deprotonated $Ag_{44}(p\text{-MBA})_{30}^{4-}$ NC-SCs is therefore in agreement with thermodynamic predictions. The octahedral SCs may be considered as a "polymorph" of the previously reported rhombohedral SCs.[2b] It is noteworthy that H-bond assisted polymorphism is a common observation in molecular crystals.[13]

Several independent observations confirmed that the octahedral SCs were formed by assimilation of $Ag_{44}(p\text{-MBA})_{30}^{4-}$ NCs in the presence of Cs^+. First, after redissolution in water (containing 66 mM CsOH for NC stability considerations, see below), the SCs showed a UV/Vis absorption spectrum (Figure 1b) that was identical to that of discrete $Ag_{44}(p\text{-MBA})_{30}^{4-}$ NCs (Figure S1a), suggesting that the size and the structure of the $Ag_{44}(p\text{-MBA})_{30}^{4-}$ NCs

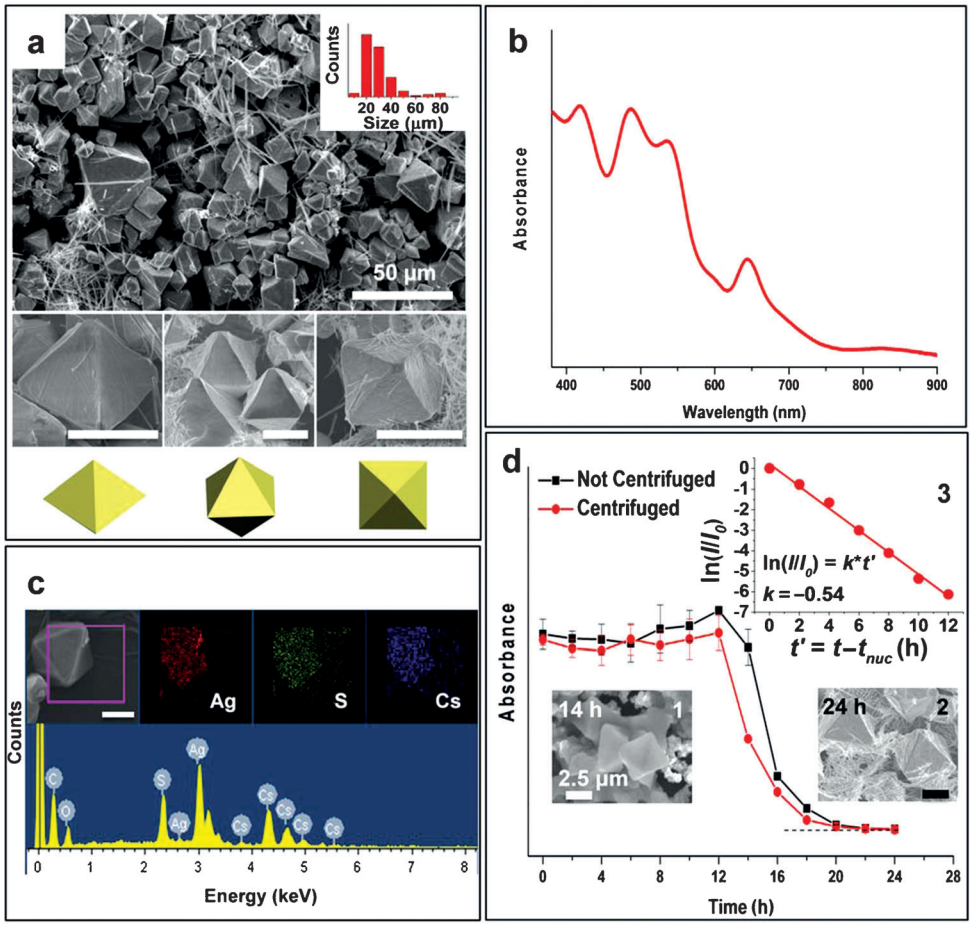

Figure 1. a) FESEM image, b) UV/Vis absorption spectrum, and c) EDX elemental analysis of octahedral SCs grown at [Cs^+] = 33 mM and X_{DMSO} = 0.5. d) UV/Vis absorbance spectrum at λ = 645 nm (I) of the crystallization solution before (black line) and after (red line) centrifugation plotted against the evaporation time (t). The top inset in (a) shows the size histogram of the SCs, whereas the bottom insets show the FESEM images and schematic illustrations of the SCs viewed from three different directions. The upper and lower panels in (c) are the elemental maps and the EDX spectrum, respectively. Insets 1 and 2 in (d) show the FESEM images of SCs harvested at different times (t), and inset 3 shows the fit of a kinetic model for the precipitation reaction of $Ag_{44}(p\text{-MBA})_{30}^{4-}$ NCs, where t_{nuc} = 12 h was used for the fitting. All scale bars in the FESEM images are 10 μm unless indicated otherwise.

were preserved in the SCs. Additional supporting evidence was obtained by energy-dispersive X-ray spectroscopy (EDX) analysis. First, all of the elements identified in the EDX spectrum (Figure 1c, lower panel) were those of the $Ag_{44}(p\text{-MBA})_{30}^{4-}$ NCs and Cs^+ cations. Quantitative analysis yielded an atomic ratio of Au/S/Cs = 1:0.68:0.76, which is consistent with completely Cs^+-deprotonated NCs with the molecular formula $Cs_4Ag_{44}(SPhCOOCs)_{30}$ (calculated atomic ratio: Au/S/Cs = 1:0.68:0.77). Furthermore, the elemental maps of a typical octahedral SC (Figure 1c, top panel) show uniform distributions of Ag (red), S (green), and Cs (blue) in the SC. Taken together, UV/Vis spectroscopy and EDX measurements indicate the conservation of shape and size of the $Ag_{44}(p\text{-MBA})_{30}^{4-}$ NCs in the octahedral SCs.

To gain insights into the crystallization process, we monitored the crystallization by following [NC] as a function of the evaporation time (t). The characteristic absorbance of the $Ag_{44}(p\text{-MBA})_{30}^{4-}$ NCs at $\lambda = 645$ nm (denoted as I) was used as a measure for [NC]. Two sets of I–t plots for the crystallization solutions before (black line) and after (red line) centrifugation (5000 rpm, 3 min) are shown in Figure 1d. The purpose of centrifugation was to remove any small SCs suspended in the crystallization solution. The solutions before and after centrifugation both showed nearly time-invariant I values at the early stage of evaporation, with plateaus in the I–t plot. The I values before and after centrifugation are also very similar. These observations indicate that the $Ag_{44}(p\text{-MBA})_{30}^{4-}$ NCs existed as discrete particles at this stage. After the plateau ($t \approx 12$ h), the I values started to decrease exponentially with time, and the I values before and after centrifugation also became more and more different, especially in the early stages of the decline ($t = 14$ h). This signals the start of the formation of small SCs, as confirmed by FESEM analysis (Figure 1d, inset 1) at $t = 14$ h where small octahedral SCs (several μm in size) were observed. After $t =$ 14 h, the I values before and after centrifugation continued to decrease, but gradually approached each other again, suggesting the settling and the growth of SCs in size. A typical FESEM image corresponding to well-grown octahedral SCs is shown in Figure 1d, inset 2 for ease of comparison.

The I–t measurements suggest that the crystallization of NCs probably occurred through a nucleation growth process (Scheme 1).[14] In the early stages of evaporation ($t < 12$ h, Phase 0 in Route I; Scheme 1), the change in solvent polarity was not sufficient to induce the crystallization of $Ag_{44}(p\text{-MBA})_{30}^{4-}$ NCs, and hence the $Ag_{44}(p\text{-MBA})_{30}^{4-}$ NCs remained in the solution phase (the I plateau in the I–t plot). However, as the decrease in polarity continued with time owing to the evaporation of water, the solubility of the $Ag_{44}(p\text{-MBA})_{30}^{4-}$ NCs ($[NC]_S$) would eventually be exceeded, and supersaturation of $Ag_{44}(p\text{-MBA})_{30}^{4-}$ NCs (as measured by $S = [NC]/[NC]_S$) occurred in the solution. When the S value was high enough (the critical value, S_{cri}) to overcome the energy barrier for nucleation, the nucleation of SCs became possible. This is the nucleation phase of the crystallization (Phase I in Route I; Scheme 1). As nucleation is usually completed within a short period of time, it is difficult to accurately identify the nucleation phase in the I–t plot. However, based on the observation of extensive formation of small SCs at $t = 14$ h, we expect the nucleation time (t_{nuc}) to be between 12 and 14 h. The octahedral shape of these small SCs also suggests that the nuclei of the SCs were also octahedral. After nucleation, the SC growth phase occurred ($t > t_{nuc}$, Phase II in Route I; Scheme 1); the SCs grew by uniform deposition of newly precipitated NCs on the surface of the growing nuclei. The depletion of discrete $Ag_{44}(p\text{-MBA})_{30}^{4-}$ NCs was more gradual in the growth phase, as shown by the decay of I at $t > t_{nuc}$.

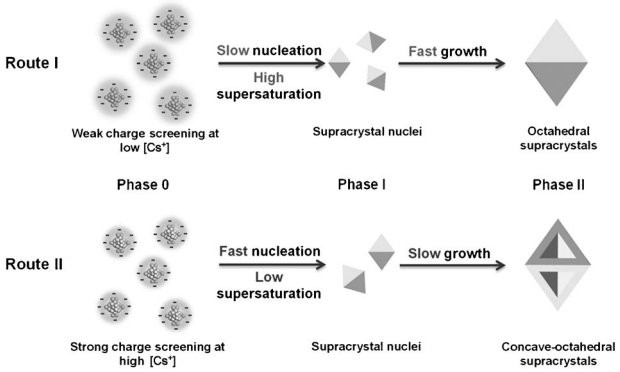

Scheme 1. Formation of octahedral (Route I) and concave-octahedral (Route II) $Ag_{44}(p\text{-MBA})_{30}^{4-}$ NC-SCs.

With the above understanding, it should be possible to modify the shape of SCs by manipulating the kinetics of their growth. We have learned from the synthesis of nanocrystals that concave faces could be developed on a polyhedral nanocrystal by selectively depositing newly formed atoms on the high-curvature sites (edges and corners).[15] Selective deposition is facilitated by a low rate of generation of the depositing atoms. We recently applied this principle (a kinetic control strategy) to program the spatial arrangement of the constituent nanocrystals in heterogeneous noble-metal nanocrystals.[15] We expect that the strategy will also work for the shape engineering of $Ag_{44}(p\text{-MBA})_{30}^{4-}$ NC-SCs. The precipitation kinetics of $Ag_{44}(p\text{-MBA})_{30}^{4-}$ NCs in the growth solution should be the equivalence of the atom-generation kinetics in nanocrystal synthesis, which is a key factor for shape engineering. As deprotonated $Ag_{44}(p\text{-MBA})_{30}^{4-}$ NCs carry a high charge (34 e^- per NC, where 30 e^- originate from the deprotonation of the p-MBA ligands and 4 e^- from the charge in the core),[2b] we hypothesized that the precipitation kinetics of $Ag_{44}(p\text{-MBA})_{30}^{4-}$ NCs could therefore be manipulated by the selective screening of the charge of the $Ag_{44}(p\text{-MBA})_{30}^{4-}$ NCs.

We therefore carried out the crystallization of $Ag_{44}(p\text{-MBA})_{30}^{4-}$ NCs under a strong charge-screening environment created by elevating $[Cs^+]$ while keeping other conditions the same. As shown in Figure 2a, the shape of the $Ag_{44}(p\text{-MBA})_{30}^{4-}$ NC-SCs changed from octahedral to concave-octahedral after increase $[Cs^+]$ from 33 to 66 mM. These concave-octahedral SCs were morphologically similar to octahedral SCs except for a distinct depression on each face and a slightly larger size (average size = 34.15 μm, the histogram of the size distribution is shown in Figure 2a, top inset). The chemical identity of the concave-octahedral SCs was

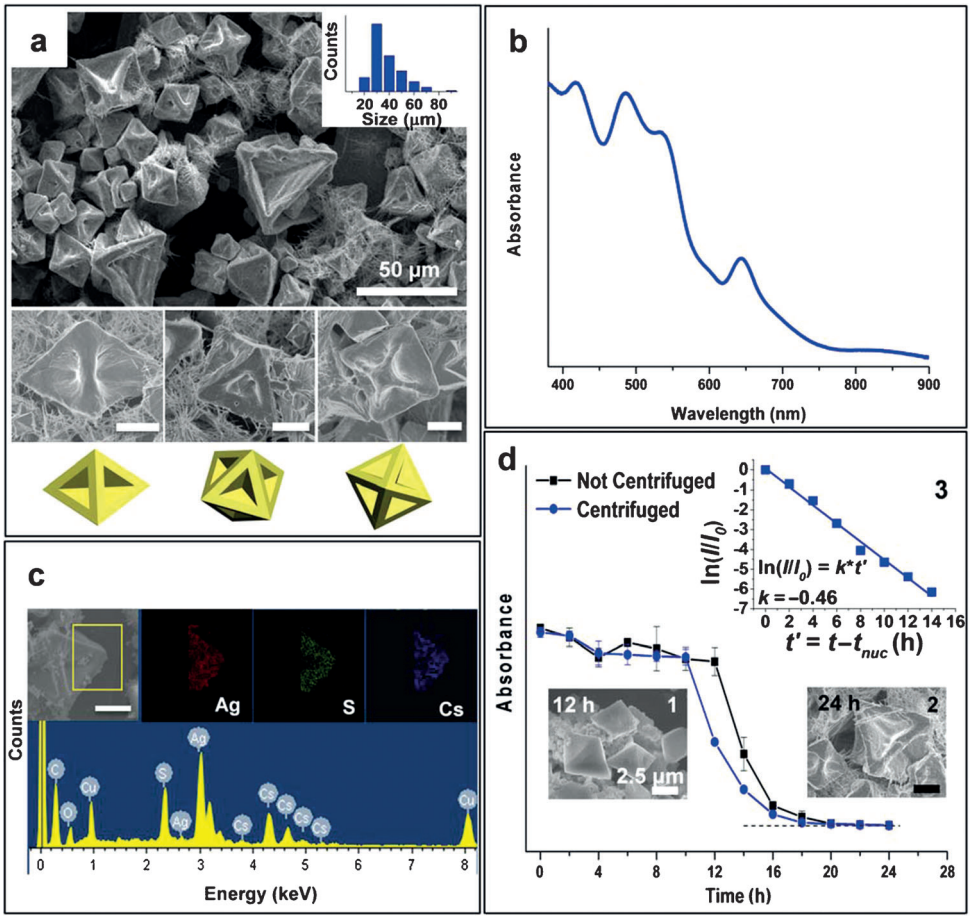

Figure 2. a) FESEM image, b) UV/Vis absorption spectrum, and c) EDX elemental analysis of concave-octahedral SCs grown at $[Cs^+]=66$ mM and $X_{DMSO}=0.5$. d) UV/Vis absorbance spectrum at $\lambda=645$ nm (I) of the crystallization solution before (black line) and after (blue line) centrifugation plotted against the evaporation time (t). The top inset in (a) shows the size histogram of SCs, whereas the bottom insets show the FESEM images and schematic illustrations of the SCs viewed from three different directions. The upper and lower panels in (c) are elemental maps and an EDX spectrum, respectively. Insets 1 and 2 in (d) show the FESEM images of SCs obtained at different t, and inset 3 shows the fit of a kinetic model for the precipitation reaction of $Ag_{44}(p\text{-MBA})_{30}^{4-}$ NCs, where $t_{nuc}=10$ h was used for the fitting. All scale bars in the FESEM images are 10 μm unless indicated otherwise.

similarly characterized by UV/Vis spectroscopy and EDX elemental analysis. The redissolved SCs (in 66 mM CsOH aqueous solution) showed identical UV/Vis absorption features (Figure 2b) to those of discrete $Ag_{44}(p\text{-MBA})_{30}^{4-}$ NCs (Figure S1a). Elemental analysis (Figure 2c, top panel) also confirmed the uniform distribution of Ag (red), S (green), and Cs (blue) throughout the concave-octahedral SCs. All elements except for Cu (from the copper grid in EDX analysis; Figure 2c, bottom panel) could be assigned to the $Ag_{44}(p\text{-MBA})_{30}^{4-}$ NCs and Cs^+ cations.

The I–t plots in Figure 2d suggest that the growth of the concave-octahedral SCs was dependent on charge-screening-assisted nucleation. The I–t plots of the concave-octahedral SCs before and after centrifugation are visually similar to those of octahedral SCs, but there are a few important differences. The most noticeable difference is an earlier onset of the divergence of I before and after centrifugation ($t=12$ h for the concave-octahedral SCs vs. 14 h for the octahedral SCs). This suggests that the nucleation of concave-octahedral SCs was kinetically more facile ($t_{nuc}=10$–12 h) because of the stronger charge screening at $[Cs^+]=66$ mM. As shown in Route II of Scheme 1 (Phase 0), the more compressed double layer of $Ag_{44}(p\text{-MBA})_{30}^{4-}$ NCs at $[Cs^+]=66$ mM improved the approach of neighboring NCs and hence increased the tendency for aggregation (nucleation). The relative lowering of the energy barrier of nucleation enabled nucleation to occur at a lower S_{cri}, which translated to a shorter evaporation time (Phase I in Route II; Scheme 1). A direct consequence of the precipitation of $Ag_{44}(p\text{-MBA})_{30}^{4-}$ NCs at lower S_{cri} was a slower precipitation kinetics (Phase II in Route II; Scheme 1). This was confirmed by the analysis of the decay kinetics of the I profile during the growth phases of both octahedral and concave-octahedral SCs (insets 3 in Figure 1d and 2d, respectively). The value of I after centrifugation was used in the kinetic analysis as it is a more accurate measure of [NC]. In both cases, the exponential decay of the I value followed pseudo-first-order kinetics, $\ln(I/I_0)=k\times(t-t_{nuc})$, where k is the specific rate constant, and I_0 denotes the absorbance at t_{nuc}. The calculated k values were 0.54 (with a coefficient of determination (R^2) of 0.993) and 0.46 ($R^2=0.989$) for the growth of octahedral SCs (Figure 1d, inset 3) and concave-octahedral SCs (Figure 2d, inset 3), respectively, confirming the slower intrinsic kinetics for the precipitation of $Ag_{44}(p\text{-MBA})_{30}^{4-}$ NCs. The slower rate of precipitation promoted the preferential deposition of newly precipitated $Ag_{44}(p\text{-MBA})_{30}^{4-}$ NCs onto the corners and edges of pre-existing nuclei to form the concave-octahedral SCs. The parallelism between the kinetic control of selective deposition in the synthesis of SCs and the kinetic control of selective deposition in the synthesis of concave-polyhedral nanocrystals has therefore been established.[16]

The corner/edge-selective deposition on octahedral SCs was also validated by FESEM analysis. The size and morphology of small SCs obtained at $t=12$ h, when the I values before and after centrifugation began to diverge, were examined by FESEM analysis (Figure 2d, inset 1). These small SCs were octahedral (several micrometers in

size) with slightly concave faces. The extent of depression in the faces was markedly lower than that of the fully developed concave-octahedral SCs (Figure 2d, inset 2). This is a good indication that the face concavity of concave-octahedral SCs was developed by the selective deposition of newly precipitated $Ag_{44}(p\text{-MBA})_{30}^{4-}$ NCs on the corners and edges of octahedral nuclei.

It should be mentioned that the charge-screening-assisted nucleation mechanism requires a suitably low S value in the starting solution to take effect. The S value in the starting solution could be controlled by X_{DMSO}. We found that octahedral SCs were the only crystallization product over a broad $[Cs^+]$ range of 16.5 to 99 mM (Figure S4b–j and f–m) at $X_{DMSO} = 0.6$ (> 0.5, $X_{DMSO} = 0.5$ was used in this study to produce both octahedral and concave-octahedral SCs). An initially high S value in the starting solution could easily transcend the range of S values suitable for corner/edge-selective deposition. In such cases, the precipitation kinetics was fast regardless of the $[Cs^+]$ value, favoring the formation of octahedral SCs. Furthermore, it was found that $[Cs^+]$ should be within a certain range of values for crystallization to occur. Extreme $[Cs^+]$ values (too high or too low) spoiled the crystallization process. For example, at a very high $[Cs^+]$ of 132 mM (at $X_{DMSO} = 0.6$), the NCs were not soluble in the starting solution under ambient conditions. The very strong charge-screening effects led the NCs to aggregate randomly into an amorphous film (for the morphology, see Figure S4k,n; the chemical analysis is given in Figure S9). At the other extreme of very low $[Cs^+]$ (8.25 mM), a rod-like assembly of NCs was observed (Figure S4a,e). The rod-like assembly was assimilated and aligned by decomposition products [mainly Ag^I–(p-MBA) complexes] of the $Ag_{44}(p\text{-MBA})_{30}^{4-}$ NCs (for a discussion on their chemical identity, see Figure S9 and S10). The decomposition of $Ag_{44}(p\text{-MBA})_{30}^{4-}$ NCs at low $[Cs^+]$ (Cs^+ provided by CsOH dissociation) could be due to their instability in the more acidic environment (Figure S11) not ramped up by CsOH. It should be mentioned that a similar alignment of Au^I–SR complexes into a one-dimensional (1D) assembly has been observed before.[17]

We have also undertaken a preliminary survey of the operating regions for the shape engineering of the $Ag_{44}(p\text{-MBA})_{30}^{4-}$ NC-SCs in the DMSO/water dual-solvent system. We mapped out the $[Cs^+]$–X_{DMSO} space as these two parameters have the greatest influence on SC formation (Figure 3). FESEM images corresponding to each dotted point in the diagrams of Figure 1, 2, and S3–S8 were taken. The diagram thus constructed can be divided into four regions (Figure 3). Two of them are suitable for SC formation, namely the upper-left region (II) for concave-octahedral SCs and the middle valley region (III) for octahedral SCs. A loose but simple rule of thumb for SC shape engineering is that high $[Cs^+]$ and low X_{DMSO} values favor the formation of concave-octahedral SCs, whereas the reverse conditions (low $[Cs^+]$ and high X_{DMSO}) favor the formation of octahedral SCs. On the other hand, experimental settings falling into the other two regions [regions I and IV] would not produce SCs. Region I is mainly due to the low stability of the $Ag_{44}(p\text{-MBA})_{30}^{4-}$ NCs in the CsOH-deficient low pH environment as discussed before. In this region, $Ag_{44}(p\text{-MBA})_{30}^{4-}$ NCs would readily decompose. The alignment of the fragments of decomposed $Ag_{44}(p\text{-MBA})_{30}^{4-}$ NCs gives rise to rod-like assemblies in this region. Region IV is defined by the solubility limit of the $Ag_{44}(p\text{-MBA})_{30}^{4-}$ NCs in the starting solution at ambient conditions where solubility is limited by either a strong charge-screening effect (owing to high $[Cs^+]$) or the low polarity of the solvent (high X_{DMSO}). The fast aggregation of $Ag_{44}(p\text{-MBA})_{30}^{4-}$ NCs in this region results in the formation of an amorphous film.

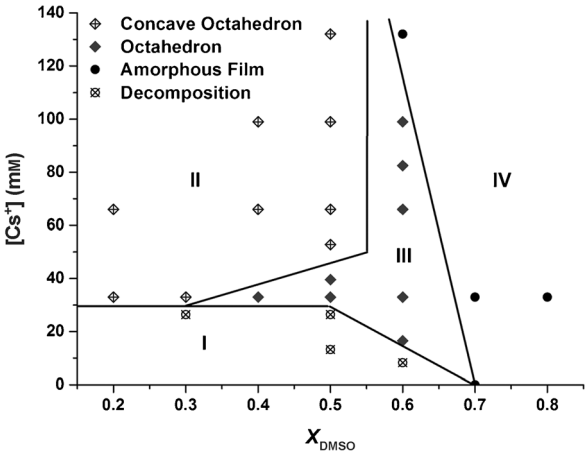

Figure 3. The operating regions of the shape-tailorable crystallization of $Ag_{44}(p\text{-MBA})_{30}^{4-}$ NCs in mixtures of DMSO and water with varied X_{DMSO} and $[Cs^+]$ values.

In summary, we have developed a simple and reproducible counterion-assisted dual-solvent method for packing $Ag_{44}(p\text{-MBA})_{30}^{4-}$ NCs into both octahedral and concave-octahedral SCs. The octahedral $Ag_{44}(p\text{-MBA})_{30}^{4-}$ NC-SCs may be regarded as a polymorph of the previously reported rhombohedral SCs. The polymorphism was caused by the elimination of the directional hydrogen bonds in the SC assembly. This was experimentally implemented by changing the counterions in the p-MBA ligands from H^+ to Cs^+. The charge-screening effect of an increased $[Cs^+]$, which altered the double-layer characteristics of the deprotonated $Ag_{44}(p\text{-MBA})_{30}^{4-}$ NCs, was highly effective in tailoring the growth kinetics of the SCs. Through the delicate control of the growth kinetics, we were able to create concavity on the exposed faces of the octahedral nuclei to form concave-octahedral SCs. We have also mapped the operating regions in the $[Cs^+]$–X_{DMSO} space to guide the shape-tailorable crystallization of $Ag_{44}(p\text{-MBA})_{30}^{4-}$ NCs. To the best of our knowledge, this is the first report of systematizing the shape engineering of NC-SCs. The simplicity and good experimental reproducibility suggest that the counterion-assisted dual-solvent approach may also be useful for the crystallization of other metal NCs.

Received: August 29, 2014
Revised: October 1, 2014
Published online: November 5, 2014

Keywords: nanoclusters · noble metals · self-assembly · shape control · supracrystals

[1] a) R. Jin, *Nanoscale* **2010**, *2*, 343 – 362; b) Z. Luo, V. Nachammai, B. Zhang, N. Yan, D. T. Leong, D.-e. Jiang, J. Xie, *J. Am. Chem. Soc.* **2014**, *136*, 10577 – 10580; c) Y. Yu, Z. Luo, D. M. Chevrier, D. T. Leong, P. Zhang, D.-e. Jiang, J. Xie, *J. Am. Chem. Soc.* **2014**, *136*, 1246 – 1249; d) X. Yuan, B. Zhang, Z. Luo, Q. Yao, D. T. Leong, N. Yan, J. Xie, *Angew. Chem. Int. Ed.* **2014**, *53*, 4623 – 4627; *Angew. Chem.* **2014**, *126*, 4711 – 4715; e) M. A. MacDonald, D. M. Chevrier, P. Zhang, H. Qian, R. Jin, *J. Phys. Chem. C* **2011**, *115*, 15282 – 15287; f) S. Chen, R. S. Ingram, M. J. Hostetler, J. J. Pietron, R. W. Murray, T. G. Schaaff, J. T. Khoury, M. M. Alvarez, R. L. Whetten, *Science* **1998**, *280*, 2098 – 2101; g) Z. Tang, D. A. Robinson, N. Bokossa, B. Xu, S. Wang, G. Wang, *J. Am. Chem. Soc.* **2011**, *133*, 16037 – 16044; h) H. Chong, P. Li, S. Wang, F. Fu, J. Xiang, M. Zhu, Y. Li, *Sci. Rep.* **2013**, *3*, 3214.

[2] a) P. D. Jadzinsky, G. Calero, C. J. Ackerson, D. A. Bushnell, R. D. Kornberg, *Science* **2007**, *318*, 430 – 433; b) A. Desireddy, B. E. Conn, J. Guo, B. Yoon, R. N. Barnett, B. M. Monahan, K. Kirschbaum, W. P. Griffith, R. L. Whetten, U. Landman, T. P. Bigioni, *Nature* **2013**, *501*, 399 – 402; c) H. Yang, Y. Wang, H. Huang, L. Gell, L. Lehtovaara, S. Malola, H. Häkkinen, N. Zheng, *Nat. Commun.* **2013**, *4*, 2422.

[3] a) M. Zhu, C. M. Aikens, F. J. Hollander, G. C. Schatz, R. Jin, *J. Am. Chem. Soc.* **2008**, *130*, 5883 – 5885; b) C. Zeng, H. Qian, T. Li, G. Li, N. L. Rosi, B. Yoon, R. N. Barnett, R. L. Whetten, U. Landman, R. Jin, *Angew. Chem. Int. Ed.* **2012**, *51*, 13114 – 13118; *Angew. Chem.* **2012**, *124*, 13291 – 13295; c) H. Qian, W. T. Eckenhoff, Y. Zhu, T. Pintauer, R. Jin, *J. Am. Chem. Soc.* **2010**, *132*, 8280 – 8281; d) M. W. Heaven, A. Dass, P. S. White, K. M. Holt, R. W. Murray, *J. Am. Chem. Soc.* **2008**, *130*, 3754 – 3755; e) D. Crasto, S. Malola, G. Brosofsky, A. Dass, H. Häkkinen, *J. Am. Chem. Soc.* **2014**, *136*, 5000 – 5005.

[4] a) Y. Xia, Y. Xiong, B. Lim, S. E. Skrabalak, *Angew. Chem. Int. Ed.* **2009**, *48*, 60 – 103; *Angew. Chem.* **2009**, *121*, 62 – 108; b) A. R. Tao, S. Habas, P. Yang, *Small* **2008**, *4*, 310 – 325; c) H. Chen, L. Shao, Q. Li, J. Wang, *Chem. Soc. Rev.* **2013**, *42*, 2679 – 2724; d) H. Chen, X. Kou, Z. Yang, W. Ni, J. Wang, *Langmuir* **2008**, *24*, 5233 – 5237.

[5] a) Y. Yu, Q. Zhang, B. Liu, J. Y. Lee, *J. Am. Chem. Soc.* **2010**, *132*, 18258 – 18265; b) J. Xie, J. Y. Lee, D. I. C. Wang, Y. P. Ting, *ACS Nano* **2007**, *1*, 429 – 439; c) C. Gao, Z. Lu, Y. Liu, Q. Zhang, M. Chi, Q. Cheng, Y. Yin, *Angew. Chem. Int. Ed.* **2012**, *51*, 5629 – 5633; *Angew. Chem.* **2012**, *124*, 5727 – 5731; d) J. Huang, Y. Zhu, M. Lin, Q. Wang, L. Zhao, Y. Yang, K. X. Yao, Y. Han, *J. Am. Chem. Soc.* **2013**, *135*, 8552 – 8561; e) H. Liu, F. Ye, Q. Yao, H. Cao, J. Xie, J. Y. Lee, J. Yang, *Sci. Rep.* **2014**, *4*, 3969; f) Y. Sun, Y. Xia, *Science* **2002**, *298*, 2176 – 2179; g) C. Susut, Y. Tong, *Electrocatalysis* **2011**, *2*, 75 – 81.

[6] a) A. Das, T. Li, K. Nobusada, C. Zeng, N. L. Rosi, R. Jin, *J. Am. Chem. Soc.* **2013**, *135*, 18264 – 18267; b) C. Zeng, T. Li, A. Das, N. L. Rosi, R. Jin, *J. Am. Chem. Soc.* **2013**, *135*, 10011 – 10013; c) Y. Levi-Kalisman, P. D. Jadzinsky, N. Kalisman, H. Tsunoyama, T. Tsukuda, D. A. Bushnell, R. D. Kornberg, *J. Am. Chem. Soc.* **2011**, *133*, 2976 – 2982.

[7] C. J. Lanci, C. M. MacDermaid, S.-g. Kang, R. Acharya, B. North, X. Yang, X. J. Qiu, W. F. DeGrado, J. G. Saven, *Proc. Natl. Acad. Sci. USA* **2012**, *109*, 7304 – 7309.

[8] a) O. C. Compton, F. E. Osterloh, *J. Am. Chem. Soc.* **2007**, *129*, 7793 – 7798; b) N. Goubet, J. Richardi, P.-A. Albouy, M.-P. Pileni, *Adv. Funct. Mater.* **2011**, *21*, 2693 – 2704; c) M. P. Pileni, *Acc. Chem. Res.* **2008**, *41*, 1799 – 1809; d) E. Auyeung, T. Li, A. J. Senesi, A. L. Schmucker, B. C. Pals, M. O. de la Cruz, C. A. Mirkin, *Nature* **2014**, *505*, 73 – 77.

[9] B. Yoon, W. D. Luedtke, R. N. Barnett, J. Gao, A. Desireddy, B. E. Conn, T. Bigioni, U. Landman, *Nat. Mater.* **2014**, *13*, 807 – 811.

[10] a) O. M. Bakr, V. Amendola, C. M. Aikens, W. Wenseleers, R. Li, L. Dal Negro, G. C. Schatz, F. Stellacci, *Angew. Chem. Int. Ed.* **2009**, *48*, 5921 – 5926; *Angew. Chem.* **2009**, *121*, 6035 – 6040; b) K. M. Harkness, Y. Tang, A. Dass, J. Pan, N. Kothalawala, V. J. Reddy, D. E. Cliffel, B. Demeler, F. Stellacci, O. M. Bakr, J. A. McLean, *Nanoscale* **2012**, *4*, 4269 – 4274.

[11] a) K. J. M. Bishop, C. E. Wilmer, S. Soh, B. A. Grzybowski, *Small* **2009**, *5*, 1600 – 1630; b) L. V. Woodcock, *Nature* **1997**, *385*, 141 – 143; c) F. Oosawa, S. Asakura, *J. Chem. Phys.* **1954**, *22*, 1255 – 1255.

[12] a) J. K. Mackenzie, A. J. W. Moore, J. F. Nicholas, *J. Phys. Chem. Solids* **1962**, *23*, 185 – 196; b) B. E. Sundquist, *Acta Metallurgica* **1964**, *12*, 67 – 86.

[13] a) L. Yu, G. A. Stephenson, C. A. Mitchell, C. A. Bunnell, S. V. Snorek, J. J. Bowyer, T. B. Borchardt, J. G. Stowell, S. R. Byrn, *J. Am. Chem. Soc.* **2000**, *122*, 585 – 591; b) C. B. Aakeröy, K. R. Seddon, *Chem. Soc. Rev.* **1993**, *22*, 397 – 407; c) G. R. Desiraju, *J. Am. Chem. Soc.* **2013**, *135*, 9952 – 9967.

[14] V. K. LaMer, R. H. Dinegar, *J. Am. Chem. Soc.* **1950**, *72*, 4847 – 4854.

[15] a) Y. Yu, Q. Zhang, J. Xie, J. Y. Lee, *Nat. Commun.* **2013**, *4*, 1454; b) Y. Yu, Q. Zhang, Q. Yao, J. Xie, J. Y. Lee, *Chem. Mater.* **2013**, *25*, 4746 – 4756.

[16] a) M. Jin, H. Zhang, Z. Xie, Y. Xia, *Angew. Chem. Int. Ed.* **2011**, *50*, 7850 – 7854; *Angew. Chem.* **2011**, *123*, 7996 – 8000; b) C.-L. Lu, K. S. Prasad, H.-L. Wu, J.-a. A. Ho, M. H. Huang, *J. Am. Chem. Soc.* **2010**, *132*, 14546 – 14553.

[17] Y. X. Zhang, H. C. Zeng, *Adv. Mater.* **2009**, *21*, 4962 – 4965.

